Received: 5 January 2023 | Revised: 10 May 2023 | Accepted: 10 June 2023

DOI: 10.1111/clr.14118

ORIGINAL ARTICLE

CLINICAL ORAL IMPLANTS RESEARCH WILEY

Influence of abutment macro- and micro-geometry on morphologic and morphometric features of peri-implant connective tissue

Luigi Canullo[1] | Alessandra Giuliani[2] | Michele Furlani[2] | Maria Menini[1] | Adriano Piattelli[3,4,5,6] | Giovanna Iezzi[7]

[1]Unit of Prosthodontics and Implant Prosthodontics, Department of Surgical Sciences (DISC), University of Genova, Genova, Italy

[2]Section BBF, Department of Clinical Sciences (DiSCO), Polytechnic University of Marche, Ancona, Italy

[3]Dental School, University of Belgrade, Belgrade, Serbia

[4]School of Dentistry, Saint Camillus International University of Health and Medical Sciences, Rome, Italy

[5]Fondazione Villa Serena per la Ricerca, Città Sant'Angelo, Italy

[6]Casa di Cura Villa Serena del Dott. L. Petruzzi, Città Sant'Angelo, Italy

[7]Department of Medical, Oral and Biotechnological Sciences, University G. d'Annunzio of Chieti-Pescara, Chieti, Italy

Correspondence
Michele Furlani, Section BBF, Department of Clinical Sciences (DiSCO), Polytechnic University of Marche, Via Brecce Bianche 1, 60131 Ancona, Italy.
Email: m.furlani@pm.univpm.it

Abstract

Objectives: The aim of the present human observational study is to provide morphologic and morphometric analysis of peri-implant connective tissue next to abutments with divergent or convergent macro-geometry and different surface micro-characteristics.

Materials and Methods: Thirty patients were rehabilitated with single implants in the posterior area and one out of three different healing abutments with a one-stage technique: machined divergent abutment (DIV-MAC), machined convergent abutment (CONV-MAC) or convergent abutment with ultrathin threaded surface (CONV-UTM). At 3 months postimplant insertion, peri-implant soft tissue was harvested; the following outcomes were investigated: histomorphometry (vertical width of connective and epithelial components) as detected by histology and polarized light; and connective tissue vertical width and 3D organization as detected by synchrotron-based high-resolution phase-contrast-based tomography (PhC-μCT).

Results: Significant differences in connective tissue vertical dimension (aJE-AM) were found between DIV-MAC and both CONV-MAC and CONV-UTM, both by histology and PhC-μCT, with significantly higher values for the last two groups. Moreover, 2D histological analysis did not find significant differences in the junctional epithelium vertical dimension (PM-aJE). Importantly, PhC-μCT analysis revealed, at 3D level, significant greater amount and density of collagen bundles for CONV-UTM compared with the other two groups.

Conclusions: Convergent abutment profiles, regardless of their surface micro-geometry, seem to favor axial development of peri-implant connective tissue. Moreover, ultrathin threaded surfaces seem associated with denser and greater connective tissue organization, which might improve peri-implant soft tissue seal.

KEYWORDS
collagen bundles, convergent abutment, divergent abutment, optical microscopy, peri-implant soft tissues, synchrotron imaging, ultrathin threaded surfaces

1 | INTRODUCTION

It has been shown that different features of osseointegrated dental implants, such as (1) macro-morphology including thread design, body shape, and neck design; (2) micro-surface morphology with the presence of grooves; and (3) implant-abutment connection with diameter mismatch (commonly known as platform shifting or platform switching) may significantly influence clinical performance and the health and response of the surrounding hard and soft tissues (Gracis et al., 2020).

Peri-implant soft tissues are formed during the wound-healing processes: After implant insertion, mucosa healing consists of the formation of an epithelium and an adaptation of the connective tissue toward the implant surface (Berglundh et al., 2019). In particular, the connective component has been demonstrated to represent a biological seal crucial to prevent down-growth of bacterial biofilm (Rodríguez et al., 2012), with vertical dimensions of 1–1.5 mm, both in animals (Abrahamsson et al., 1996; Berglundh & Lindhe, 1996) and humans (Tomasi et al., 2013). Its establishment and maintenance were acknowledged as key factors for implant success (Rompen et al., 2006; Salvi et al., 2015; Schroeder & Listgarten, 1997).

The implant surface's chemical and topographic properties seem to be of relevance for the biological response of the surrounding tissues (Menini et al., 2015; Sanz-Sánchez et al., 2018) during the healing process (Mangano et al., 2018; Mariotti & Hefti, 2015; Wennerberg et al., 2003). For instance, micro-grooved surfaces were associated with longer connective tissue attachment and minor bone resorption around implants (Iglhaut et al., 2014). In agreement with these findings, some studies have recently shown that modified prosthetic abutment surfaces promote the creation of more robust collagen networks attached to abutments at early stages (Nevins et al., 2012; Shapoff et al., 2016). However, too rough surfaces at the soft tissue level could speed up bacterial growth (Quirynen et al., 1993), enhancing the risk for plaque-induced inflammatory reactions in surrounding tissues (i.e., mucositis) which may induce peri-implantitis lesion with loss of marginal bone (Pesce et al., 2014).

More recently, coronally convergent shapes of transmucosal components were shown to favor peri-implant tissue healing and maintenance over time (Canullo et al., 2022; Canullo, Menini, et al., 2021).

In particular, regarding the neck design, a systematic review with meta-analysis (Valente et al., 2020), considering the impact of concave/convergent versus parallel/divergent implant transmucosal profiles on hard and soft peri-implant tissues, revealed that, while concave/convergent implant transmucosal profiles result in less marginal bone loss, no statistically significant differences were obtained for soft tissue-related outcomes nor for the platform-matching connection subgroup.

Our hypothesis is that the lack of statistically significant information on soft tissue-related outcomes could be linked to the fact that almost all of the previous studies were exclusively based on two-dimensional (2D) morphological investigations, mainly cross-sectional histological analysis. In order to fully understand the extent and the distribution of the peri-implant connective tissue, it is helpful to resort to three-dimensional (3D) imaging techniques, capable of reconstructing the 3D structural complexity of the collagen bundles. In this context, some of the authors recently showed (Iezzi et al., 2021), by high-resolution synchrotron-based phase-contrast imaging, that peri-implant connective tissue presents transverse and longitudinal oriented collagen bundles, intertwining with each other; thus, they demonstrated that synchrotron imaging is capable of studying 3D parameters that cannot be analyzed with histologic techniques but are important to define the 3D micro-architecture of the collagen bundles and the 3D structural complexity of the connective tissue (i.e., to quantify connective tissue anisotropy degree and connectivity density).

We also hypothesized that due to the forces existing at the interface between implant and connective tissue, it is essential to discriminate the directionality of the longitudinal neck profile from its curvature: Therefore, it is necessary to study neck profiles that are equal in shape and volume, with a straight profile, that is, neither concave nor convex, but with opposite macro-geometry, that is, with converging versus diverging vertical profiles.

Thus, we included in the present study abutments with divergent straight necks (DIVergent MAChined/DIV-MAC) and also convergent straight necks (CONVergent MAChined/CONV-MAC and CONVergent Ultrathin Threaded Microsurface/CONV-UTM) with the same macro-geometry (same shape and same volume). The UTM convergent abutments had the same macro-geometry but an increased micro-surface, that is, roughness, respect to the CONV-MAC group. Considering these three experimental groups, the variables that differentiate the various experimental groups were minimized, bringing out only possible differences between the three groups attributable to the directionality of the normal forces exerted by and on the collagen bundles.

On this basis, the aim of the present human observational study was to provide morphologic and morphometric analysis of peri-implant connective tissue next to abutments with divergent or convergent macro-geometry and different surface micro-characteristics, reconstructing the organization of the connective tissue with high reliability.

2 | MATERIALS AND METHODS

2.1 | Patient selection and study design

The study was designed as an experimental investigation on humans including patients requiring single implant supported restoration in the posterior upper or lower sectors.

All patients (demographic and clinical data were summarized in Table 1) signed an informed consent and the permission of the Human Investigation Committee was granted (Nr.881, Prot.N429/Ethics Committee Lazio 1, April 21st 2022).

The patients were treated with one out of three different healing abutment macro-/micro-geometries: 30 surgical samples of soft tissue around abutments were tested, after a healing time of 3 months. The following experimental groups were considered:

- DIV-MAC group – Nr.10 DIVergent MAChined abutments
- CONV-MAC group – Nr.10 CONVergent MAChined abutments
- CONV-UTM group – Nr.10 CONVergent Ultrathin Threaded Microsurface abutments

The three groups had an identical macro-surface of the abutment, but the CONV-UTM group also presented a micro-grooved surface. MAC surface was constituted by circular micro-threads with depth lower than 2 μm, Sa mean value of 0.2 and Ra of 0.11; conversely, UTM surface presented a threading with a triangular profile and pitch >50 μm, Sa mean value of 0.6 and Ra of 0.62. Schematic draws of the divergent (DIV) and convergent (CONV) macro-designs were reported in Figure 1a,b, respectively. Moreover, scanning electron microscopy images of the different micro-geometries, smooth (MAC) and tridimensional (UTM), were shown in Figure 1c,d, respectively.

The outcomes were assessed by the following measurements:

1. Primary outcome

Measurement of the total vertical dimension of the mucosa, as well as of connective and epithelial components in height by histology-based morphometric analysis. The vertical dimension of connective portion was complementary measured by synchrotron imaging-based morphometric analysis.

1. Secondary outcomes

- Qualitative 2D evaluation of collagen bundles orientation by polarized light microscopy;
- Quantitative 3D evaluation of peri-implant collagen 3D organization by synchrotron-based high-resolution phase-contrast tomography.

2.2 | Inclusion/exclusion criteria

The following inclusion criteria were considered:

- Patient requiring single implant supported restoration of the posterior area;
- Residual alveolar bone width of edentulous jaw >8 mm;
- Keratinized mucosa width >6 mm;
- Males and females between 18 and 80 years old;
- Patients with healthy periodontal conditions (Treated periodontitis, Plaque Index [PI] <25%, and Bleeding on Probing [BoP] <25%);

TABLE 1 Demographic and clinical patient data.

	Age, mean (SD)	Sex, (M/F)	Biotype, (thin/thick)	Gingival height (<3/>3)	BoP (0/1/2/3/4)	PI (0/1/2/3/4)
DIVergent MAC	61.6 (8.83)	6/4	4/6	4/6	7/2/0/1	4/5/1/0
CONVergent MAC	56.9 (8.61)	3/7	4/6	4/6	8/1/0/1	6/4/0/0
CONVergent UTM	57.8 (5.98)	3/7	4/6	4/6	7/2/0/1	5/4/1/0
Aggregates	58.7 (7.91)	12/18	12/18	12/18	22/5/0/3	15/13/2/0

Abbreviations: BoP, bleeding on probing; PI, plaque index.

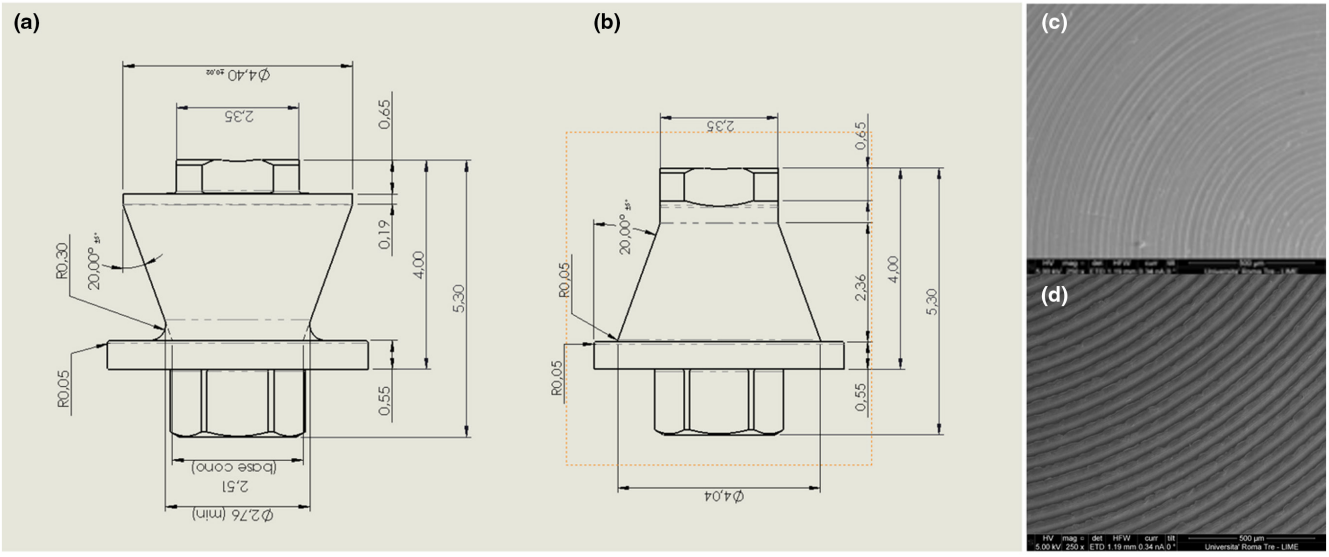

FIGURE 1 Schematic draw of the different macro-designs: (a) divergent, (b) convergent. SEM images of the different surfaced included in the study; (c) smooth, MAC; (d) tridimensional, UTM. Courtesy Sweden & Martina.

- Patients that are willing to sign an informed consent and participate in a clinical study;
- Generally fit and healthy and able to undergo oral surgical procedures under local anesthesia.

Moreover, teeth at the surgical site which required removal were extracted a minimum of 12 weeks prior to sinus floor elevation; this choice deals with the fact that the physiological rearrangement of the postextraction site requires at least 3–4 months.

Exclusion criteria were as follow:

- Patients who smoke over 10 cigarettes/day
- Pregnancy (confirmed by verbal inquiry)
- Chronic systemic pathologies (e.g., diabetes) and neoplasia of the Oro-Facial District
- Patients taking bisphosphonates
- Any sites where an implant already failed
- Untreated periodontitis
- Dental sites with acute infections
- Chronic inflammatory diseases of the oral cavity
- Autoimmune diseases (cortisone intake)
- Allergy declared to one or more medicaments to be used during treatment
- Alcoholic patients and/or drug addicts
- History or malignant tumors of the maxillary sinus
- History of radiation therapy of the head and neck area.

Furthermore, all patients were without systemic disorders, had no history of periodontal disease, and were nonsmokers (only two of them were smokers with less than 10 cig/day).

2.3 | Sample size calculation

A similar histologic study aiming to study soft tissue integration with different abutment surfaces (Canullo, Penarrocha Oltra, et al., 2021) reported a power analysis conducted with the G*Power software (version 3.1.9.7) and revealed that 9 abutments would have produced a power of 96.7% of detecting a significant difference of standardized effect size (Cohen's *d*) 1.76 with an alpha error set to 0.05. Thus, 30 abutments were included, 10 for each experimental group.

In synchrotron imaging investigation, due to their 3D nature, the morphometric parameters derived from the stacking of more than 3500 successive 2D sections (each with a thickness of about 890 nm), mapping the entire connective portion of the sample. This is of paramount importance because it allowed us to perform this observatory experiment based on a small (30) number of patients but obtaining results of extreme reliability and statistical significance. This method, in case of animal model studies, can reduce to the minimum the number of the sacrifices, in full respect of the ethical international rules (3Rs principles).

2.4 | Clinical procedures

All patients underwent demographic and medical questioning, mouth cleaning, clinical evaluation, and received oral hygiene instructions at least 2-weeks before surgery. All the patients received an antibiotic prescription according to Caiazzo et al. (2021): one shot amoxicillin and clavulanic acid 1 h before surgery. The patients were treated under local anesthesia using Lidocaine + epinephrine 1:100,000. At the time of primary surgery, following a computer guided implant insertion, one endosseous implant (Premium ONE, Sweden & Martina, Padua, Italy) was installed with a one-stage approach. An especially designed titanium abutment was inserted presenting one of the following macro-/micro- geometries: divergent machined (DIV-MAC), convergent machined (CONV-MAC), and convergent ultrathin threaded micro-surface (CONV-UTM). Sutures 6.0 (Polynil, Sweden & Martina, Italy) were used to adapt flaps for primary intention on the abutment and a tension-free soft tissue closure was achieved. Postoperative management including systemic antibiotics, anti-inflammatory drugs, and salt water mouth rinsing (for 10 days) was prescribed.

The one-stage approach was used to minimize the number of surgeries for the patient. Additionally, this approach is supposed to be used in case of simple (no need of GBR) cases, such as the ones included in the present study.

Three months after implant insertion, clinical examination and periapical X-rays were performed, and tested abutments were removed through a special mucotome allowing the harvesting of 1 mm of soft peri-implant tissue all around the abutment. Impression was taken and a permanent screw retained zirconia restoration was delivered 1 week later.

2.5 | Sample processing

All biopsies (abutments with surrounding soft tissues) were fixed in 10% buffered formalin, then dehydrated in a graded series of ethanol rinses, and finally embedded in a glycolmethacrylate resin (Methyl-Methacrylate [MMA] following chemical dehydration).

Removal and subsequent polymerization of soft tissues attached to abutments allow the maintenance of the soft tissue architecture, without introducing bias, that is, without altering their dimensions and features (Iezzi et al., 2021).

After polymerization, the abutments embedded in resin blocks were sectioned along their longitudinal axis in order to obtain two portions (portions 1 and 2 in Figure 2). Portion 1 was handled by traditional methods and cut with Precise 1 (Automated System; Assing). The tissue/abutment half incorporated in resin and intended for synchrotron analysis (portion 2 in Figure 2) was mounted in a clamp and subsequently viewed under microscope (Leica Wild M3Z Stereo Zoom Microscope) to highlight the soft tissue/abutment interface. Subsequently, a thin scalpel was inserted into the interface; afterwards, through a lever action, the abutment was detached from the

FIGURE 2 Abutment surrounded by soft tissues and embedded in resin blocks were sectioned along their longitudinal axis in order to obtain two portions. Portion 1 was used to obtain the longitudinal sections to the major axis of the abutment; afterwards, the sample slices were stained by toluidine blue and acid fuchsin. Portion 2 was examined by synchrotron radiation imaging, after removal of the abutment; afterwards, it was sectioned along its transversal axis for evaluation under a polarized light microscope.

block. It is important that the included metal part is no more than 2 mm thick and that there are no undercuts.

Overall, the tissue samples were prepared using the methods described by Berglundh et al. (1994, 2007) and by Thomsen and Ericson (1985).

The slices were stained by toluidine blue and acid fuchsin.

2.6 | Histology

Histological analysis was carried out under a light microscope (Laborlux S; Leitz) connected to a high-resolution video camera (3CCD, JVCKY-F55B; JVC) and interfaced with a PC. This optical system was associated with a digitizing pad (Matrix Vision GmbH) and a histomorphometry software package with image capturing capabilities (Image-Pro Plus 4.5; Media Cybernetics Inc., Immagini & Computer Snc). The histological images were performed at 40× and 100× magnification to carry out the histological evaluations. One single well-trained examiner, not involved in the surgical treatment, evaluated the histological results. A code was reported on the histological slides so that no indications were available on the abutment features. The following histological landmarks were identified in each section:

- margin of the peri-implant mucosa (PM)
- apical extension of the junctional epithelium (aJE)
- apical location of the mucosal part (AM).

The vertical distance between the landmarks was measured by analyzing the projections of the points on a line parallel to the long axis of the abutment ("height" dimension).

Therefore, the margin of the peri-implant mucosa (PM), the apical extension of the barrier epithelium (aJE), and the apical location of the abutment (AM) were identified (Figure 3a).

The evaluation of the vertical dimension of the connective tissue (CT) constituted the outcome measurement; in addition, the vertical dimension of the overall soft tissues (PM-AM) and of the junctional epithelium (JE) at the implant-mucosal interface were evaluated.

2.7 | Polarized light

Birefringence allowed to highlight the transverse orientation of the collagen by polarized light microscopy. Collagen fibers were viewed by placing thin sections of tissue under an Axiolab light microscope (Laborlux S; Leitz) equipped with two linear polarizers and two quarter wave plates arranged to have a transmitted circularly polarized light. Collagen fibers aligned perfectly transverse to the direction of the light propagation (parallel to the plane of the section) appeared bright due to a change in the refraction of existing light, whereas the collagen fibers aligned along the axis of light propagation (perpendicular to the plane of the section) appeared with different color because no refraction occurred.

2.8 | Phase-contrast-based tomography

The high-resolution phase-contrast-based tomography (PhC-μCT) was performed at the SYRMEP beamline of the ELETTRA Synchrotron Radiation Facility (Basovizza, TS, Italy). In agreement with previous studies (Iezzi et al., 2021), because of the synchrotron X-ray wavefield high coherence characteristics, we investigated the index of refraction $n = 1 - \delta + i\beta$ and, in particular, the electron density related to the phase shift term δ.

The scans were performed using the beam provided by the ELETTRA facility (2 GeV, 300 mA); beam filter: 1 mm Silicon; average energy: 19.3 keV; exposure time per projection: 0.4 s; 3600 projections over a total range of 360°; sample-detector distance: 100 mm; pixel size: 890 nm.

Tomographic reconstructions were performed using the SYRMEP Tomo Project (STP) open-source software (Brun et al., 2017). The Paganin's method was applied to retrieve the phase contrast signal (Paganin et al., 2002); the δ/β ratio was set to 100.

For each biopsy, a longitudinal sequence of subvolumes was investigated, from the apical location to the margin of the peri-implant mucosa; each subvolume had a fixed dimension of $540 \times 270 \times 270\,\mu m^3$ and had the longest side as close as possible to the interface with the abutment. Four parameters were extracted: connective tissue height (Conn.Tissue Height – expressed in mm); connective tissue-specific volume (Conn.Tissue SpV – expressed in %); connective tissue degree of anisotropy (Conn.Tissue DA); and connective tissue connectivity density (Conn.Tissue ConnD – expressed in $pixel^{-3}$). The Conn.Tissue

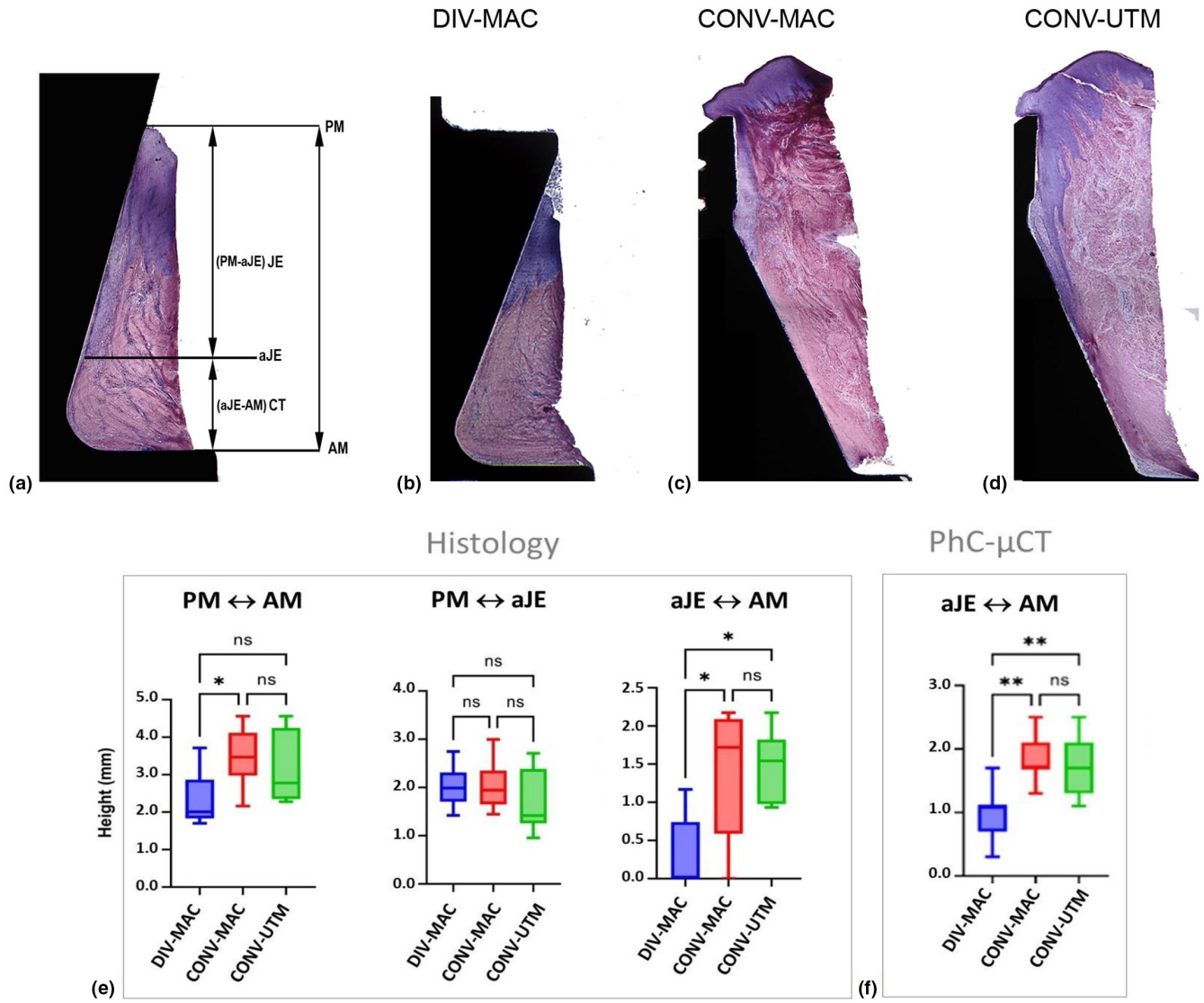

FIGURE 3 (a) Illustration of the histological measurements. The margin of the peri-implant mucosa (PM), the apical extension of the junctional epithelium (aJE), and the apical location of the abutment (AM) were identified. The evaluation of the total vertical dimension of the soft tissues (PM-AM), the junctional epithelium (JE) and connective tissue (CT) of the implant-mucosal interface were evaluated; (b) histological section of the DIV-MAC abutment (toluidine blue and acid fuchsin, 18×); (c) histological section of the CONV-MAC abutment (toluidine blue and acid fuchsin, 18×); (d) histological section of the CONV-UTM abutment (toluidine blue and acid fuchsin, 18×). (e, f) Histologic and Synchrotron Imaging Data Analysis: box-and-whisker diagram of the distribution of vertical height dimensions. (e) Histomorphometric evaluation of the total vertical dimension of the soft tissues (PM ↔ AM), of the junctional epithelium (JE: PM ↔ aJE) and of the connective tissue (CT: aJE ↔ AM) in the implant-mucosal interface; (f) 3D Synchrotron morphometric evaluation of the connective portion (CT: aJE ↔ AM). Comparisons between the three experimental groups (i.e., DIV-MAC, CONV-MAC, CONV-UTM). Upper and lower ends of boxes represent 75th and 25th percentiles. The median value is showed with a solid line. $^{*}p < .05$, $^{**}p < .01$.

Height is the vertical distance that was measured in a direction that was parallel to the long axis of the abutment; the Conn.Tissue SpV is the ratio between the collagen voxels volume and the total volume of the investigated tissue; the Conn.Tissue DA measures the similarity of a structure to a uniform distribution and varies between 0, corresponding to perfect isotropy, and 1, representing all collagen bundles confined to a single plane or axis; finally, the Conn.Tissue ConnD is a morphometric descriptor for the interconnectivity of the collagen bundles: High values correspond to better-connected collagen bundles, that is, more entangled peri-implant connective tissues, while low values are related to poorly connected ones, that is, more lax peri-implant connective tissues.

In particular, before segmentation and limitedly to the Conn. Tissue DA and the Conn.Tissue ConnD analysis, a fixed pipeline was adopted: (1) median filter: 2.0; (2) Sobel filter (Find Edges function in Fiji); and (3) Enhance Contrast: 0.30%, with Equalize histogram flagged. For the Conn.Tissue SpV parameter, only the median filter (2.0) has been applied before segmentation.

The full morphometric analysis was performed using the BoneJ Plugin-ImageJ v3 software. The 3D reconstructions and videos

were generated using Dragonfly v2022.1 software (Object Research Systems [ORS] Inc, 2020).

2.9 | Statistical methods

Descriptive statistics and differences between experimental groups were analyzed using the software package Prism 6.0 (GraphPad Software). The null hypothesis of no difference between groups was rejected at $p < .05$. Data distributions were checked for normality by Kolmogorov–Smirnov and Shapiro–Wilk tests, homogeneity of variances by Levene test. The parameters showing normality and homogeneity of variance between groups were evaluated using one-way ANOVA and Tukey's multiple comparisons test; otherwise, the groups were tested using the nonparametric Kruskal–Wallis one-way ANOVA on Ranks and Dunn's multiple comparisons test.

The nonparametric Spearman correlation coefficients *R* were calculated for the complete set of synchrotron parameters.

3 | RESULTS

3.1 | Histological analysis

Twenty-four abutments were histologically examined: 9 DIV-MAC, 8 CONV-MAC, and 7 CONV-UTM (6 specimens were not evaluated as they were damaged during harvesting with the mucotome). Histomorphometric analysis showed that all 24 samples exhibited peri-implant mucosa lining the abutment profile. In some samples, a small gap was found between the connective tissue and the abutment profile. Tissue maturation and collagen fibers organization were evident after 3 months of healing; moreover, the formation of junctional epithelium (JE) was well represented in all samples. A layer of fibroblasts formed the connective tissue interface to titanium. In connective tissue (CT), few vascular structures were found. In some cases, mild inflammatory infiltrates were present and they were interposed between the collagen fibers.

3.1.1 | Divergent machined (DIV-MAC)

Four out of 9 samples of the peri-implant mucosa presented with JE that was continuous with CT in the mucosal portion that formed the interface toward the apical portion of the abutment (Figure 3b). In contrast, the other 5 samples showed a junctional epithelium that occupied all the tissue facing the abutment surface.

3.1.2 | Convergent machined (CONV-MAC)

Most of the samples (7 out of 8) had well-defined barrier epithelium that continued with an organized portion of CT in the median and/or apical portion of the sample (Figure 3c).

3.1.3 | Convergent ultrathin threaded microsurface (CONV-UTM)

All samples had a well-defined barrier epithelium that continued with an organized portion of CT in the median and/or apical portion of the sample (Figure 3d).

The mean vertical dimensions of the mucosa are reported in Table 2 and Figure 3e. The Kruskal–Wallis test, applied because normality was not verified for all the experimental groups, showed significant differences in PM↔AM height and in aJE↔AM connective height among the three experimental groups (Table 2). In particular, Dunn's multiple comparisons test indicated differences in aJE↔AM connective height between the DIV-MAC and both CONV-MAC and CONV-UTM groups, with significantly higher values for the last two groups. Moreover, Dunn's multiple comparisons test also indicated differences in PM↔AM height between the DIV-MAC and CONV-MAC groups, with significantly higher values for the last group. We did not observe significant differences in the PM↔aJE height of epithelial tissue among the three groups.

3.2 | Polarized light analysis

The polarized light showed a distribution of the collagen bundles that was distinguishable both in longitudinal and transverse sections. Collagen bundles were more recognizable near the implant surface, while they were less organized in the most far portion.

Furthermore, in the samples in which the entire soft tissue-abutment interface was occupied by JE, the distribution of fibers was not regular.

3.2.1 | Longitudinal sections

Closer to the implant surface, it was observed that collagen fibers followed the macro-geometry of the abutment. In the DIV-MAC samples, the collagen fibers had a horizontal course in the most apical portion of the abutment while their course became oblique in the divergent portion (Figure 4a). In contrast, in the CONV groups (MAC and UTM), the collagen fibers followed the convergent slope of the abutment in both groups (Figure 4b,c).

3.2.2 | Transversal sections

The collagen fibers running perpendicular to the longitudinal axis of the implant showed semicircular orientations (they ran around the circular profile of the abutment finishing their way by anchoring themselves to the oral epithelium).

In the DIV-MAC abutment, the transverse bundles appear to be thinner than the CONV groups (MAC and UTM) indeed they formed less evident intersection areas (Figure 4d,e).

TABLE 2 Histologic landmarks in peri-implant soft tissues of the three experimental groups.

Kruskal–Wallis test				
Landmarks	**DIV-MAC[a]**	**CONV-MAC[a]**	**CONV-UTM[a]**	***p***
PM ↔ AM (height)	**2.3 ± 0.3, 2.0**	**3.5 ± 0.3, 3.5**	**3.2 ± 0.4, 2.8**	**.0084**
PM ↔ aJE (height)	2.0 ± 0.1, 2.0	2.0 ± 0.2, 1.9	1.7 ± 0.3, 1.4	.4799
aJE ↔ AM (height)	**0.3 ± 0.2, 0.0**	**1.4 ± 0.3, 1.7**	**1.5 ± 0.2, 1.5**	**.0042**
Dunn's multiple comparisons test				
Groups	**Histological landmarks**	**Mean (mm)**		***p***
DIV-MAC vs. CONV-MAC	PM ↔ AM (height)	**2.3 vs. 3.5**		**.0132**
DIV-MAC vs. CONV-UTM		2.3 vs. 3.2		.0537
CONV-MAC vs. CONV-UTM		3.5 vs. 3.2		>.9999
DIV-MAC vs. CONV-MAC	PM ↔ aJE (height)	2.0 vs. 2.0		>.9999
DIV-MAC vs. CONV-UTM		2.0 vs. 1.7		.9133
CONV-MAC vs. CONV-UTM		2.0 vs. 1.7		.8133
DIV-MAC vs. CONV-MAC	aJE ↔ AM (height)	**0.3 vs. 1.4**		.0144
DIV-MAC vs. CONV-UTM		**0.3 vs. 1.5**		.0144
CONV-MAC vs. CONV-UTM		1.4 vs. 1.5		>.9999

Note: Statistically significant values ($p < .05$) in bold.

Abbreviations: aJE, apical extension of the barrier epithelium; AM, apical location of the abutment; PM, margin of the peri-implant mucosa.

[a]Mean ± SE, median values (mm).

3.3 | PhC-μCT and data analysis

Thirty biopsies were included in the Synchrotron imaging program, 10 for each experimental group; however, 8 samples presented problems during sample processing or cutting and therefore were excluded. Hence, 22 abutments were examined: 8 DIV-MAC, 7 CONV-MAC, and 7 CONV-UTM.

Full biopsies were investigated for each patient obtaining 3D-imaging and morphometric mapping of the whole peri-implant connective tissue in the three experimental groups.

The height (axial direction of the implant) of the peri-implant connective tissue (Conn.Tissue height – mm) was measured in the area closest to the interface with the abutment, that is, within a radial maximum distance from the interface of about 300–400 μm. These results are reported in Figure 3f and Table 3. The one-way ANOVA test, applied because normality and homogeneity of variances were verified, showed differences among the three experimental groups (Table 3). In particular, Tukey's multiple comparisons test indicated differences between the DIV-MAC group and both CONV-MAC and CONV-UTM groups, with significantly higher values for these last two groups.

Moreover, to compare amount and 3D distribution of collagen in the three experimental groups, the full 3D morphometric analysis was performed on the complete set of samples. Several stack-sequences of sub-volumes (each with a final volume of $540 \times 270 \times 270\,\mu m^3$, with the longest side of the prism as close as possible to the mucosa/abutment interface and mapping the complete biopsies in the longitudinal direction) have been considered and morphometrically investigated. Radially, that is, in planes transverse to the direction of the implant axis, the prisms had a maximum distance from the interface of about 300–400 μm. Vertically, that is, parallel to the direction of the axis of the implant, they were stacked one after the other until reaching, for each sample, the maximum height of the connective tissue in contact with the implant. Representative subvolumes (prisms) of the DIV-MAC, CONV-MAC, and CONV-UTM groups are reported in Figure 5a–c and Videos S1–S3, respectively. The full 3D collagen morphometric quantification, including the shape and 3D complexity analysis, is reported in Figure 5d and Table 3. For each sample, we considered subvolumes in which the amount of collagen was maximally expressed, that is, with the highest SpV values.

As regards the Conn.Tissue SpV parameter, the Kruskal–Wallis test, applied because equivariance was not verified, showed differences among the three experimental groups (Table 3). In particular, Dunn's multiple comparisons test indicated differences between the DIV group and CONV-UTM, with a significantly higher value for the last group.

As regards the Conn. Tissue DA parameter, the ordinary one-way ANOVA test, applied because normality and homogeneity of variances were verified, showed no differences among the three experimental groups (Table 3).

As regards the Conn.Tissue ConnD parameter, the ordinary one-way ANOVA test, applied because normality and homogeneity of variances were verified, showed no differences among the three experimental groups (Table 3). However, Tukey's multiple comparisons test indicated differences between the DIV-MAC and CONV-UTM groups ($p = .0430$), with a significantly higher value for the last group.

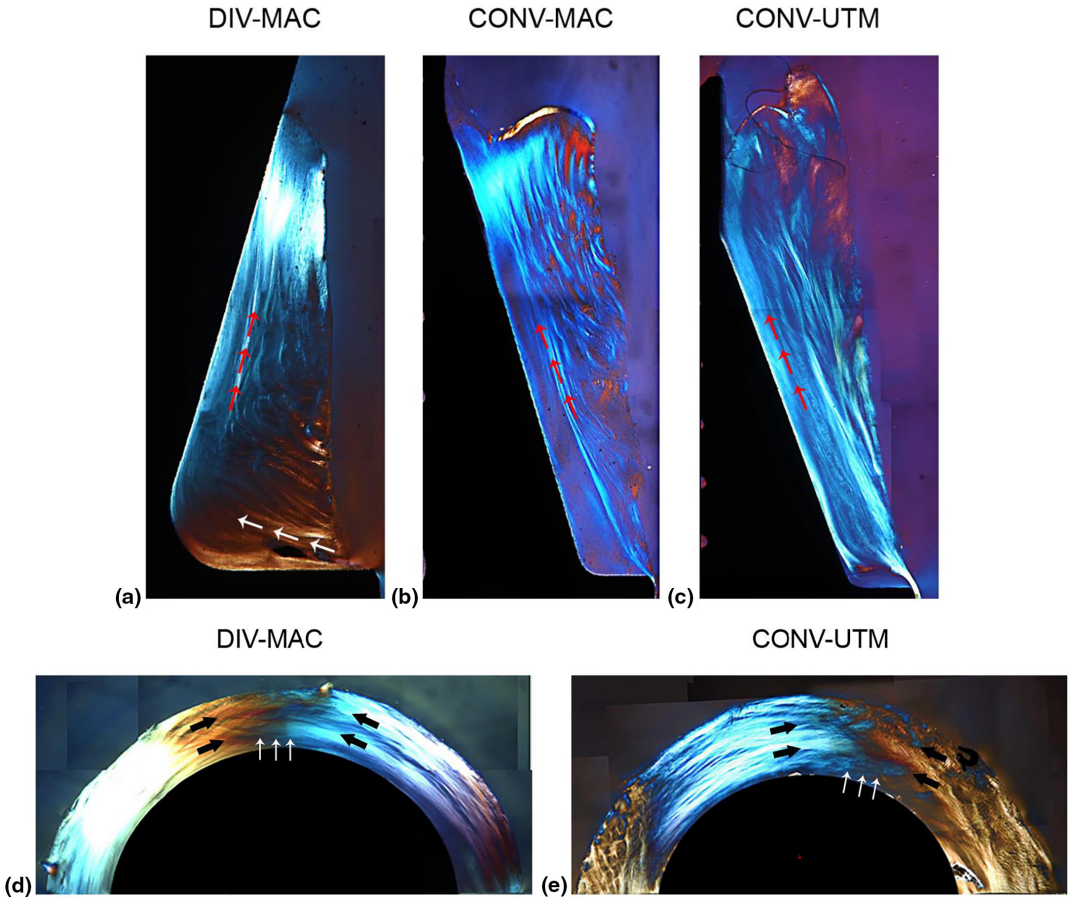

FIGURE 4 (a–c) Polarized light microscopy of the longitudinal section of the peri-abutment soft tissue. The collagen fibers orientation was found to be of different color due to the diffraction values of the polarized light plane passing throughout the section. The light blue (red arrows) indicated the collagen fibers parallel to the vertical profile of the implant–abutment unit, whereas the dark blue color showed the collagen fibers that run perpendicularly or circularly to the implant–abutment unit. (a) In the DIV-MAC abutment, the collagen fibers had an initially horizontal trend in the most apical portion of the abutment (white arrows), while their course became oblique in the divergent portion of the abutment (red arrows). (b, c) Conversely, in both converging abutments (CONV-MAC and CONV-UTM), the collagen fibers followed the convergent profile (red arrows) of the abutments in both groups. (d, e) Polarized light microscopy of the transverse reconstructions of the peri-abutment soft tissues surrounding an area ≤1/2 of the abutment circumference. Transverse collagen bundles run perpendicular to the long axis of the implant abutment unit and showed a semicircular orientation. In fact, they run around the abutment partly following its circular profile, intersecting each other during their path (white arrows). (d) In the DIV-MAC abutment, the transverse bundles appear to be thinner (black arrows), (e) while in the converging abutments (CONV-MAC and CONV-UTM), they appear to form thicker bundles (black arrows) that form more evident areas of intersection (white arrows).

Finally, the Spearman correlation coefficients were calculated for the complete set of parameters quantified by synchrotron imaging. As shown in Figure 6, the highest absolute values of *R* were in the "moderate" range. The remaining correlations were "weak" or "very weak".

4 | DISCUSSION

The morphometrical analysis demonstrated the positive effect of convergent abutment macro-geometry compared to traditional divergent ones in terms of soft tissue integration. In fact, a significantly higher connective tissue was found around convergent groups by histological analysis and confirmed by synchrotron 3D imaging.

We did not observe significant differences in the height of epithelial tissue among the three groups.

The intertwining net of collagen bundles, with semicircular transversal collagen bundles intersecting with longitudinal ones (Iezzi et al., 2021), was here confirmed in all the experimental groups.

Synchrotron analysis, together with the significant difference in connective tissue height (vertical thickness) between convergent versus divergent groups, also highlighted the significantly positive effect of the 3D micro-grooved surface (CONV-UTM) compared to the machined one (CONV-MAC) in terms of density of collagen bundles that intertwine. Indeed, connective tissue amount and connectivity were considered as independent quality factors from each other, because Spearman index showed "weak" or at most "moderate" correlations between them. Thus, micro-grooved surfaces were confirmed to enhance early fibroblast adhesion and

TABLE 3 PhC-μCT parameters in peri-implant connective tissues of the three experimental groups.

Parameter	DIV-MAC[a]	CONV-MAC[a]	CONV-UTM[a]	*p*
Conn.Tissue height (mm)	**1.0 ± 0.1, 1.1**	**1.8 ± 0.1, 1.7**	**1.7 ± 0.2, 1.7**	**.0009**[b]
Conn.Tissue SpV (%)	**84 ± 3, 84**	**88 ± 2, 88**	**94 ± 1, 95**	**.0180**[c]
Conn.Tissue DA	0.55 ± 0.07, 0.57	0.51 ± 0.05, 0.54	0.55 ± 0.05, 0.54	.8299[b]
Conn.Tissue ConnD ($\times 10^{-3}$ px^{-3})	1.8 ± 0.2, 1.8	2.1 ± 0.2, 2.1	2.5 ± 0.1, 2.4	.0533[b]
Multiple comparisons tests				
Groups	**Parameters**	**Mean**		***p***
DIV-MAC vs. CONV-MAC	Conn.Tissue height (mm)	**1.0 vs. 1.8**		**.0013**[d]
DIV-MAC vs. CONV-UTM		**1.0 vs. 1.7**		**.0053**[d]
CONV-MAC vs. CONV-UTM		1.8 vs. 1.7		.8269[d]
DIV-MAC vs. CONV-MAC	Conn.Tissue SpV (%)	84 vs. 88		>.9999[e]
DIV-MAC vs. CONV-UTM		**85 vs. 94**		**.0205**[e]
CONV-MAC vs. CONV-UTM		88 vs. 94		.2516[e]
DIV-MAC vs. CONV-MAC	Conn.Tissue DA	0.55 vs. 0.51		.8607[d]
DIV-MAC vs. CONV-UTM		0.55 vs. 0.55		.9992[d]
CONV-MAC vs. CONV-UTM		0.51 vs. 0.55		.8507[d]
DIV-MAC vs. CONV-MAC	Conn.Tissue ConnD ($\times 10^{-3}$ px^{-3})	1.8 vs. 2.1		.5444[d]
DIV-MAC vs. CONV-UTM		**1.8 vs. 2.5**		**.0430**[d]
CONV-MAC vs. CONV-UTM		2.1 vs. 2.5		.3141[d]

Note: Statistically significant values ($p < .05$) in bold.

[a]Mean ± SE, median values.

[b]Ordinary one-way ANOVA test.

[c]Kruskal–Wallis test.

[d]Tukey's multiple comparisons test.

[e]Dunn's multiple comparisons test.

activation, favoring the formation of a biological seal and promoting tissue integration. In particular, the concept of "contact guidance" (Lee et al., 2009) was quantitatively assessed. Indeed, as observed by Doyle et al. (2009), cells migrate rapidly through 3D fibrillar matrices by a 1D migratory mechanism not mimicked by 2D matrices. Moreover, the micro-patterning of CONV-UTM group is made of surfaces with wide grooves (>50 μm) that seem to be more appropriate than surfaces with narrow grooves (<50 μm) in order to avoid a fibrotic response, as suggested by Guillem-Marti et al. (2013).

These results have a significant impact in implantology: In fact, the influence of abutment macro- and micro-geometries on peri-implant tissue has been a frequent topic of research over the last decades. All previous studies were based on two-dimensional optical or electron microscopy. In this context, Hirashima et al. (2020) showed the need to use three dimensional methods when studying collagen bundles: They showed that in schemes based on observations using conventional single section methods, periodontal ligament (PDL) cells appeared spindle shape and oriented parallel to PDL fibers, while schemes based on 3-dimensional observations correctly showed that PDL cells in the horizontal fiber area are flat or wing-shaped, rather than spindle-shaped, and are arranged virtually perpendicular to PDL fibers. Moreover, 3D observations showed that PDL fibers have multiple connected branches. Therefore, since the peri-implant connective tissue is a 3D structure such as PDL fibers, the use of 3D analysis methods in addition to two-dimensional optical or electronic microscopy completes the knowledge of the soft tissue through the analysis of its organization. In fact, parameters of fundamental interest at micro-structural level, that is, those indicating the 3D structural complexity parameters (Conn.Tissue DA and Conn.Tissue Conn.D), cannot in any way be evaluated with two-dimensional methods. These parameters are very important in biomechanics because they are indicators of the directionality of the forces exerted by the connective tissue, that is, by the collagen bundles, and therefore, they can give fundamental information on the stability of the tissue itself (Karjalainen et al., 2021). Moreover, an evaluation exclusively based on the thickness of the connective tissue (vertical and/or transversal) is a not sufficient information to ensure the stability of the soft tissue. In fact, numerous studies stated that large quantities of collagen, without directionality or with uncontrolled connectivity, create dysfunctional fibrotic structures (Belloni et al., 2022; Giuliani et al., 2019; Rockey et al., 2015).

In this context, the connective tissue around dental implant abutments constitutes an interesting in vivo model to study human wound healing; indeed, well-organized connective tissues around the neck of dental implants were recently hypothesized to decrease

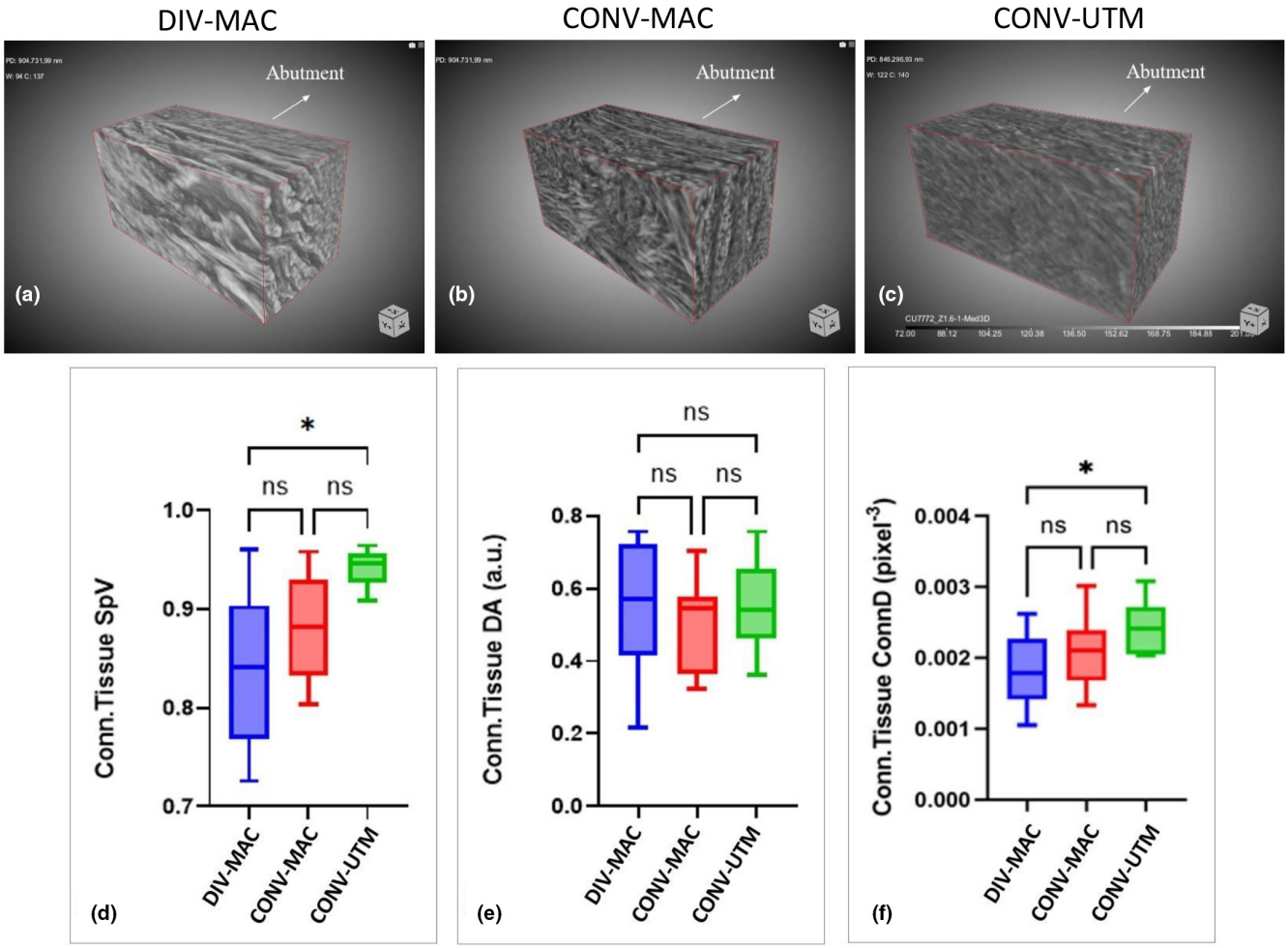

FIGURE 5 (a–c) Synchrotron 3D reconstructions of representative subvolumes (each with a fixed dimension of $540\times270\times270\,\mu m^3$ and with the longest side of the prism as close as possible to the interface with the abutment) of the (a) DIV-MAC, (b) CONV-MAC, and (c) CONV-UTM groups: The decreased contrast between collagen fibers and interstitial spaces in the CONV-UTM group is an indication of an increased amount and interlacing of the collagen bundles. (d–f) Synchrotron imaging Data Analysis. Box-and-whisker diagram of the distribution of PhC-μCT morphometric parameters: (d) connective tissue specific volume (Conn.Tissue SpV – %), (e) connective tissue anisotropy degree index (Conn.Tissue DA), and (f) connective tissue connectivity density (Conn.Tissue ConnD – pixel^{-3}). Statistical comparison among the three experimental groups (i.e., DIV-MAC, CONV-MAC, CONV-UTM). Upper and lower ends of boxes represent 75th and 25th percentiles. The median value is showed with a solid line. *$p<.05$.

early bone resorption by preventing inflammatory cell apical migration (Berglundh et al., 2019; Rodríguez et al., 2012).

This study was designed to reconstruct the 3D organization of peri-implant connective tissue in the presence of identical macro-geometries of the three experimental groups (same volume and same lateral surface) but opposite orientation of the abutment neck; in the divergent case, the abutment neck was an overturned truncated cone, in the convergent cases a straight truncated cone. We have chosen not to use concave or convex profiles (but straight ones) in order not to hide the contributions of the different profile portions in terms of forces normal to the implant profile (Figure 1a,b). This choice also allowed us to provide just height measurements, like in Tomasi et al. (2013), without referring to profile linear measurements, as performed in most studies. Indeed, the straight profile of the necks in the three experimental groups, with the same angle of inclination with respect to the bases (about 22° – Figure 1a,b), guarantees a direct proportionality between the profile and the vertical height.

However, the present study presents also some limitations: for instance, it does not fully match the clinical setting where the cyclic forces of masticatory load are present. Indeed, these loading forces add to the contact forces modifying the context. However, we preferred not to include also cyclic forces of masticatory load in this study in order to not confuse their contribution with the action of contact forces. Moreover, even if this work is focused on unloaded implants, in follow-up studies we will consider the same implants after masticatory loading and, interestingly, in the presence of immediate loading. Before including the masticatory loading forces, it is necessary to find a method that allows to discriminate the volume and organization of the transverse fibers from the longitudinal ones. The lack of such discrimination constitutes another limitation of the current study: Indeed, synchrotron imaging is fundamentally based

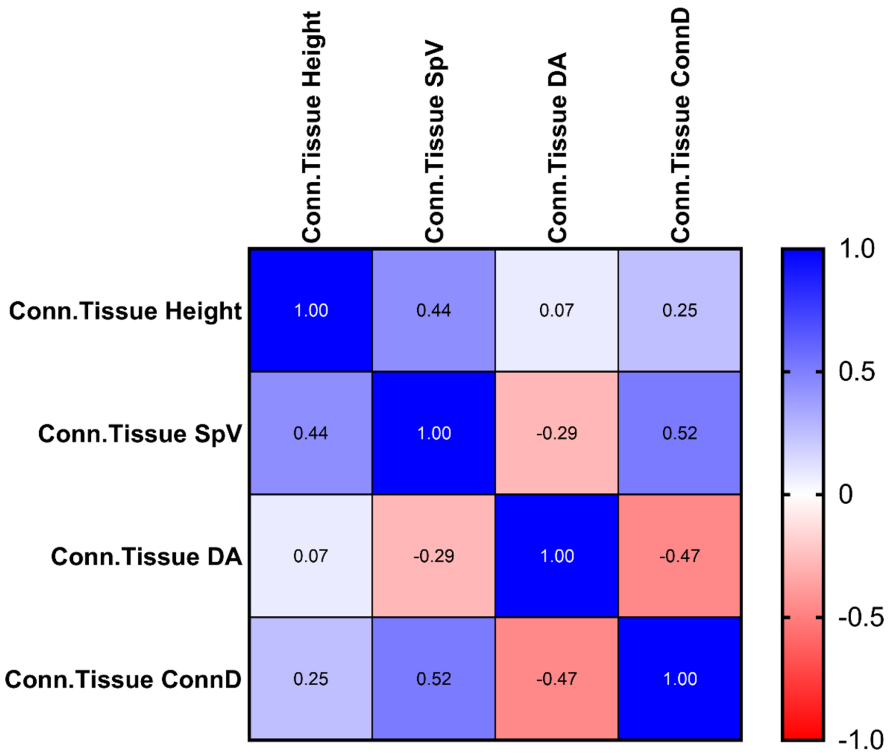

FIGURE 6 Correlation between the complete set of parameters quantified by synchrotron imaging (i.e., Conn.Tissue Height, Conn.Tissue SpV, Conn.Tissue DA, and Conn.Tissue ConnD). Spearman *R* is indicated. Correlations were considered: "very weak" in *R*-range = 0–.19;"weak" in *R*-range = .20–.39; "moderate" in *R*-range = .40–.59; "strong" in *R*-range = .60–.79; "very strong" in *R*-range = .80–1.0. The highest absolute values of *R* were in the "moderate" range (.40–.59), with a positive correlation between Conn.Tissue Height and Conn.Tissue SpV (*R* = +.44) and between Conn.Tissue ConnD and Conn.Tissue SpV (*R* = +.52), and a negative correlation between Conn.Tissue DA and Conn.Tissue ConnD (*R* = −.47).

on the detection of tissues on the basis of their different densities. Unfortunately, transversal fibers and longitudinal fibers have the same density: therefore, alternative methods of analysis are needed with respect to traditional systems based on signal thresholding. In this direction, we are developing imaging analysis methods based on artificial intelligence that can distinguish the micro-architecture of the peri-implant connective tissue not only on the basis of tissues density but also of their shape or orientation, achieving the discrimination between transverse bundles and longitudinal ones.

Here, it was shown that clinical outcomes during peri-implant wound healing are also affected by the abutment macro- and micro-geometry, most likely determining special force settings at the interfaces between soft tissues and abutment. For this reason, next studies will focus on these forces and on the stored energies at the abutment surface, for instance, introducing plasma treatments, in order to better understand boundaries between functional regenerative phenomena, fibrosis, and cancer events.

AUTHOR CONTRIBUTIONS

Canullo L. contributed to conception and design, contributed to interpretation, drafted manuscript, and critically revised manuscript; Giuliani A. contributed to design, contributed to acquisition, analysis, and interpretation, drafted manuscript and critically revised manuscript; Furlani M. contributed to design, contributed to acquisition and analysis, and drafted manuscript; Menini M. contributed to conception, contributed to interpretation, and critically revised manuscript; Piattelli A. contributed to conception, contributed to interpretation, and critically revised manuscript; Iezzi G. contributed to conception and design, contributed to acquisition, analysis, and interpretation, drafted manuscript and critically revised manuscript. All authors gave final approval and agree to be accountable for all aspects of the work.

ACKNOWLEDGMENTS

The authors acknowledge Sweden & Martina for providing all dental implants studied in this investigation. We also acknowledge Elettra Sincrotrone Trieste for providing access to its synchrotron radiation facilities and Dr. Giuliana Tromba for assistance in using beamline SYRMEP. Moreover, we acknowledge Euro-BioImaging (www.eurobioimaging.eu) for providing access to imaging technologies and services via the PCI @ Italy – Phase Contrast Imaging Flagship Node Trieste (Trieste, Italy) – experiment PID: 1611. The 3D reconstructions and Videos S1–S3 for this paper were generated using Dragonfly software, Version 2022.1 for Windows, Object Research Systems (ORS) Inc, Montreal, Canada, 2020; software available at http://www.theobjects.com/dragonfly.

CONFLICT OF INTEREST STATEMENT

The authors declared no potential conflicts of interest with respect to the research, authorship, and/or publication of this article.

DATA AVAILABILITY STATEMENT

The data that support the findings of this study are available from the corresponding author upon reasonable request.

ORCID

Michele Furlani https://orcid.org/0000-0002-9261-2682
Giovanna Iezzi https://orcid.org/0000-0002-2391-6594

REFERENCES

Abrahamsson, I., Berglundh, T., Wennström, J., & Lindhe, J. (1996). The peri-implant hard and soft tissues at different implant systems. A comparative study in the dog. *Clinical Oral Implants Research*, *7*, 212–219.

Belloni, A., Furlani, M., Greco, S., Notarstefano, V., Pro, C., Randazzo, B., Pellegrino, P., Zannotti, A., Carpini, G. D., Ciavattini, A., Di Lillo, F., Giorgini, E., Giuliani, A., Cinti, S., & Ciarmela, P. (2022). Uterine leiomyoma as useful model to unveil morphometric and macromolecular collagen state and impairment in fibrotic diseases: An ex-vivo human study. *Biochimica et Biophysica Acta – Molecular Basis of Disease*, *1868*(12), 166494.

Berglundh, T., Abrahamsson, I., Welander, M., Lang, N. P., & Lindhe, J. (2007). Morphogenesis of the peri-implant mucosa: An experimental study in dogs. *Clinical Oral Implants Research*, *18*(1), 1–8.

Berglundh, T., Jepsen, S., Stadlinger, B., & Terheyden, H. (2019). Peri-implantitis and its prevention. *Clinical Oral Implants Research*, *30*, 150–155.

Berglundh, T., & Lindhe, J. (1996). Dimension of the periimplant mucosa. Biological width revisited. *Journal of Clinical Periodontology*, *23*, 971–973.

Berglundh, T., Lindhe, J., Jonsson, K., & Ericsson, I. (1994). The topography of the vascular systems in the periodontal and peri-implant tissues in the dog. *Journal of Clinical Periodontology*, *21*(3), 189–193.

Brun, F., Massimi, L., Fratini, M., Dreossi, D., Billé, F., Accardo, A., Pugliese, R., & Cedola, A. (2017). SYRMEP Tomo project: A graphical user interface for customizing CT reconstruction workflows. *Advanced Structural and Chemical Imaging*, *3*, 1–9.

Caiazzo, A., Canullo, L., Consensus Meeting Group, & Pesce, P. (2021). Consensus report by the Italian Academy of Osseointegration on the use of antibiotics and antiseptic agents in implant surgery. *The International Journal of Oral & Maxillofacial Implants*, *36*(1), 103–105.

Canullo, L., Hjerppe, J., Menini, M., Bagnasco, F., Petazzi, G. M., & Pesce, P. (2022). Zirconia crowns and FDPs with feather-edge margins on conical implant abutments-up-to-5-year clinical retrospective study. *The International Journal of Prosthodontics*, *35*, 380–386.

Canullo, L., Menini, M., Bagnasco, F., Di Tullio, N., & Pesce, P. (2021). Tissue-level versus bone-level single implants in the anterior area rehabilitated with feather-edge crowns on conical implant abutments: An up to 5-year retrospective study. *The Journal of Prosthetic Dentistry*, *11*, S0022-3913(21)00082-2.

Canullo, L., Penarrocha Oltra, D., Pesce, P., Zarauz, C., Lattanzio, R., Penarrocha Diago, M., & Iezzi, G. (2021). Soft tissue integration of different abutment surfaces: An experimental study with histological analysis. *Clinical Oral Implants Research*, *32*(8), 928–940.

Doyle, A. D., Wang, F. W., Matsumoto, K., & Yamada, K. M. (2009). One-dimensional topography underlies three-dimensional fibrillar cell migration. *The Journal of Cell Biology*, *184*(4), 481–490.

Giuliani, A., Greco, S., Pacilè, S., Zannotti, A., Delli Carpini, G., Tromba, G., Giannubilo, S. R., Ciavattini, A., & Ciarmela, P. (2019). Advanced 3D imaging of uterine leiomyoma's morphology by propagation-based phase-contrast microtomography. *Scientific Reports*, *9*, 10580.

Gracis, S., Llobell, A., Bichacho, N., Jahangiri, L., & Ferencz, J. L. (2020). The influence of implant neck features and abutment diameter on hard and soft tissues around single implants placed in healed ridges: Clinical criteria for selection. *The International Journal of Periodontics & Restorative Dentistry*, *40*(1), 39–48.

Guillem-Marti, J., Delgado, L., Godoy-Gallardo, M., Pegueroles, M., Herrero, M., & Gil, F. J. (2013). Fibroblast adhesion and activation onto micro-machined titanium surfaces. *Clinical Oral Implants Research*, *24*(7), 770–780.

Hirashima, S., Ohta, K., Kanazawa, T., Okayama, S., Togo, A., Miyazono, Y., Kusukawa, J., & Nakamura, K. (2020). Three-dimensional ultrastructural analysis and histomorphometry of collagen bundles in the periodontal ligament using focused ion beam/scanning electron microscope tomography. *Journal of Periodontal Research*, *55*, 23–31.

Iezzi, G., Di Lillo, F., Furlani, M., Degidi, M., Piattelli, A., & Giuliani, A. (2021). The symmetric 3D organization of connective tissue around implant abutment: A key-issue to prevent bone resorption. *Symmetry*, *13*, 1126.

Iglhaut, G., Schwarz, F., Winter, R. R., Mihatovic, I., Stimmelmayr, M., & Schliephake, H. (2014). Epithelial attachment and downgrowth on dental implant abutments – A comprehensive review. *Journal of Esthetic and Restorative Dentistry*, *26*, 324–331.

Karjalainen, V. P., Kestilä, I., Finnilä, M. A., Folkesson, E., Turkiewicz, A., Önnerfjord, P., Hughes, V., Tjörnstrand, J., Englund, M., & Saarakkala, S. (2021). Quantitative three-dimensional collagen orientation analysis of human meniscus posterior horn in health and osteoarthritis using micro-computed tomography. *Osteoarthritis and Cartilage*, *29*(5), 762–772.

Lee, S. W., Kim, S. Y., Rhyu, I. C., Chung, W. Y., Leesungbok, R., & Lee, K. W. (2009). Influence of microgroove dimension on cell behaviour of human gingival fibroblasts cultured on titanium substrata. *Clinical Oral Implants Research*, *20*(1), 56–66.

Mangano, C., Mangano, F. G., Shibli, J. A., Roth, L. A., d'Addazio, G., Piattelli, A., & Iezzi, G. (2018). Immunohistochemical evaluation of peri-implant soft tissues around machined and direct metal laser sintered (DMLS) healing abutments in humans. *International Journal of Environmental Research and Public Health*, *30*, 15.

Mariotti, A., & Hefti, A. F. (2015). Defining periodontal health. *BMC Oral Health*, *15*, S6.

Menini, M., Dellepiane, E., Chvartszaid, D., Baldi, D., Schiavetti, I., & Pera, P. (2015). Influence of different surface characteristics on peri-implant tissue behavior: A six-year prospective report. *The International Journal of Prosthodontics*, *28*, 389–395.

Nevins, M., Camelo, M., Nevins, M. L., Schupbach, P., & Kim, D. M. (2012). Connective tissue attachment to laser-microgrooved abutments: A human histologic case report. *International Journal of Periodontics & Restorative Dentistry*, *32*, 385–392.

Paganin, D., Mayo, S. C., Gureyev, T. E., Miller, P. R., & Wilkins, S. W. (2002). Simultaneous phase and amplitude extraction from a single defocused image of a homogeneous object. *Journal of Microscopy*, *206*, 33–40.

Pesce, P., Menini, M., Tealdo, T., Bevilacqua, M., Pera, F., & Pera, P. (2014). Peri-implantitis: A systematic review of recently published papers. *The International Journal of Prosthodontics*, *27*, 15–25.

Quirynen, M., van der Mei, H. C., Bollen, C. M., Schotte, A., Marechal, M., Doornbusch, G. I., Naert, I., Busscher, H. J., & van Steenberghe, D. (1993). An in vivo study of the influence of the surface roughness of implants on the microbiology of supra- and subgingival plaque. *Journal of Dental Research*, *72*, 1304–1309.

Rockey, D. C., Bell, P. D., & Hill, J. A. (2015). Fibrosis – A common pathway to organ injury and failure. *The New England Journal of Medicine*, *372*(12), 1138–1149.

Rodríguez, X., Vela, X., Calvo-Guirado, J. L., Nart, J., & Stappert, C. F. (2012). Effect of platform switching on collagen fiber orientation and bone resorption around dental implants: A preliminary histologic animal study. *The International Journal of Oral & Maxillofacial Implants*, *27*, 1116–1122.

Rompen, E., Domken, O., Degidi, M., Pontes, A. E., & Piattelli, A. (2006). The effect of material characteristics, of surface topography and of implant components and connections on soft tissue integration: A literature review. *Clinical Oral Implants Research*, *17*, S55–S67.

Salvi, G. E., Bosshardt, D. D., Lang, N. P., Abrahamsson, I., Berglundh, T., Lindhe, J., Ivanovski, S., & Donos, N. (2015). Temporal sequence of hard and soft tissue healing around titanium dental implants. *Periodontology 2000*, *68*, 135–152.

Sanz-Sánchez, I., Sanz-Martín, I., Carrillo de Albornoz, A., Figuero, E., & Sanz, M. (2018). Biological effect of the abutment material on the

stability of peri-implant marginal bone levels: A systematic review and meta-analysis. *Clinical Oral Implants Research*, *18*, 124–144.

Schroeder, H. E., & Listgarten, M. A. (1997). The gingival tissues: The architecture of periodontal protection. *Periodontology 2000*, *13*, 91–120.

Shapoff, C. A., Babushkin, J. A., & Wohl, D. J. (2016). Clinical use of laser-microtextured abutments: A case series. *The International Journal of Periodontics & Restorative Dentistry*, *39*, 655–662.

Thomsen, P., & Ericson, L. E. (1985). Light and transmission electron microscopy used to study the tissue morphology close to implants. *Biomaterials*, *6*(6), 421–424.

Tomasi, C., Tessarolo, F., Caola, I., Wennstrom, J., Nollo, G., & Berglundh, T. (2013). Morphogenesis of peri-implant mucosa revisited: An experimental study in humans. *Clinical Oral Implants Research*, *3*, 1–7.

Valente, N. A., Wu, M., Toti, P., Derchi, G., & Barone, A. (2020). Impact of concave/convergent vs parallel/ divergent implant transmucosal profiles on hard and soft peri-implant tissues: A systematic review with meta-analyses. *The International Journal of Prosthodontics*, *33*(5), 553–564.

Wennerberg, A., Sennerby, L., Kultje, C., & Lekholm, U. (2003). Some soft tissue characteristics at implant abutment with different surface topography. A study in humans. *Journal of Clinical Periodontology*, *30*, 88–94.

SUPPORTING INFORMATION

Additional supporting information can be found online in the Supporting Information section at the end of this article.

How to cite this article: Canullo, L., Giuliani, A., Furlani, M., Menini, M., Piattelli, A., & Iezzi, G. (2023). Influence of abutment macro- and micro-geometry on morphologic and morphometric features of peri-implant connective tissue. *Clinical Oral Implants Research*, *34*, 920–933. https://doi.org/10.1111/clr.14118